Supplementary Information

Surface proton hopping conduction mechanism dominant polymer electrolytes created by self-assembly of bicontinuous cubic liquid crystals

Takahiro Ichikawa*[a], Takeshi Yamada*[b], Nanami Aoki[a],[‖], Yuki Maehara[a],[‖], Kaori Suda[a], and Tsubasa Kobayashi[a]

Correspondence to: t-ichi@cc.tuat.ac.jp, t_yamada@cross.or.jp

1. Materials and methods

1.1. General

All the reagents were purchased from Sigma Aldrich and Tokyo Kasei corporation. All reactions were carried out under an argon atmosphere in anhydrous solvents. **GZ** was synthesized according to the literature.[1] ^{1}H and ^{13}C nuclear magnetic resonance (NMR) spectra were recorded on a JEOL model JNM-ECA 400 spectrometer operating at 400.00 MHz and 100.00 MHz for ^{1}H and ^{13}C NMR, respectively. The thermal properties of the compounds and the polymer films were examined using a differential scanning calorimeter (DSC-6220, Seiko Instruments). A polarizing optical microscope Olympus BX51 equipped with a Linkam LK-600 hot stage was used for observing the phase behavior.

1.2. Preparation of Film-G

DMPA (2,2-Dimethoxy-2-phenylacetophenone) was selected as a photo-polymerization initiator. Homogeneous mixtures of **GZ**, HTf_2N, and DMPA were prepared by dissolving requisite amounts of the three compounds in a chloroform/methanol mixed solvent and subsequent removal of the solvent. The molar ratio between **GZ** and HTf_2N was controlled to be 1:0.5 while the weight ratio of DMPA was controlled to be 1.0 wt% against the total weight of **GZ** and HTf_2N. 18.5 wt% of water was added to the mixture and kneaded with spatula to be homogeneous. The obtained homogeneous mixtures were sandwiched by a Teflon sheet and a transparent film with 100 μm thickness spacers. UV irradiation was performed for the mixtures for 2 h at 30 °C using a xenon lamp as a light source.

1.3. Characterization of Film-G

The characterization of **Film-G** was performed in our previous study.[1] In the present study, the presence of the gyroid nanostructure was also confirmed by the same ways using polarizing optical microscope observation and X-ray diffraction measurements (Fig. S1).

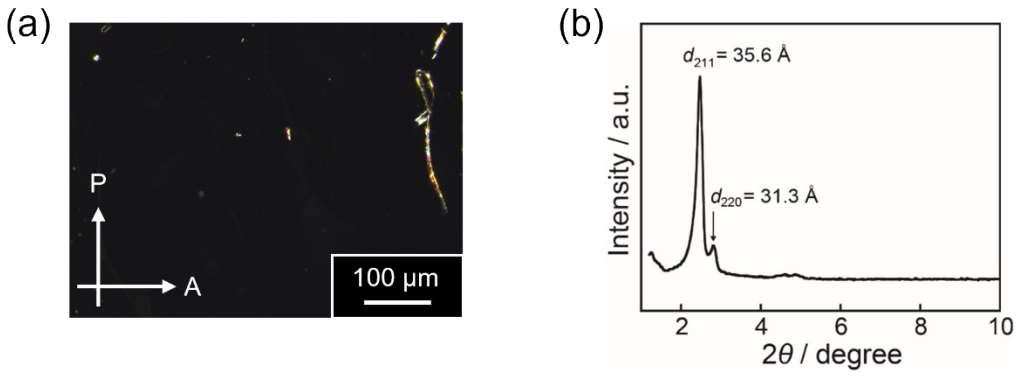

Fig. S1. (a) Polarizing optical microscope image of **Film-G** at 25 °C. (b) XRD pattern of **Film-G** at 25 °C. The observation of (211) and (220) reflections is indicative of the presence of a gyroid nanostructure.

1.4. Impedance measurement

Alternating current impedance measurements were performed using a Schlumberger Solartron 1260 impedance analyzer (frequency range = 10 Hz to 10 MHz, applied voltage = 0.1 V). Two rod-shaped gold electrodes were used for measuring ionic conductivity perpendicular to the film surface (Fig. S2). This measurement gave the proton conductivity of **Film-G** in perpendicular directions to the film surface.

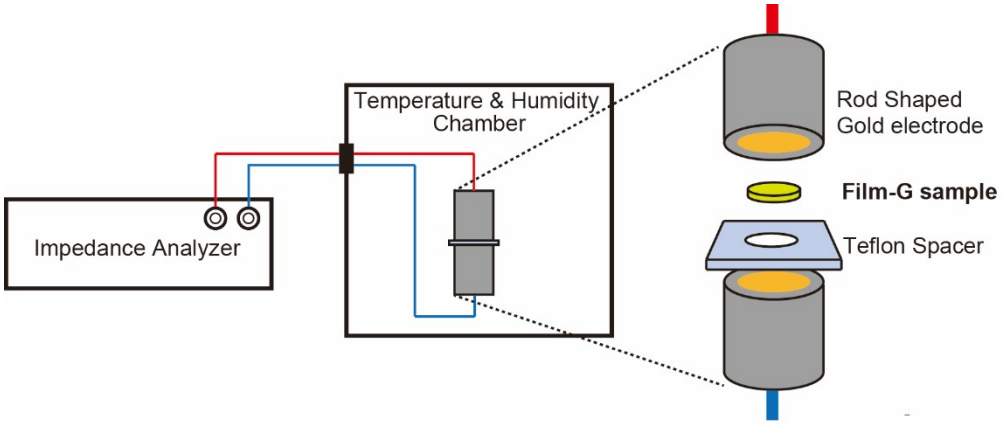

Fig. S2. Schematic representation of the electrical cell used for examining proton (ionic) conductivity.

The distance between the two electrodes (l) is 0.24 [mm] and the **Film-G** surface area (A) is 3.14 × 1.0 ×1.0 = 3.14 [mm^2]. The cell constant value is l / A = 1/3.14 = 0.0764 [mm^{-1}] = 0.764 [cm^{-1}], which was used for the calculation of σ_{H^+} values.

1.5. Quasi elastic neutron scattering (QENS) measurements

QENS measurements were performed at the BL02-DNA near-back scattering spectrometer in Materials and Life Science Experimental Facility (MLF), J-PARC (Tokai, Japan).[2,3] The energy resolution was 3.6 μeV with operating a pulse shaping chopper at 225Hz. The covered energy transfer and momentum transfer ranges are –40 to 100 μeV and 0.1 to 1.9 Å^{-1}, respectively. Four samples of **Film-G/3H_2O**, **Film-G/3D_2O**, **Film-G/6H_2O**, and **Film-G/6D_2O** were measured at 300, 280, 260, and 10 K. The data at 10 K were used for the resolution. The counting time was almost 5 hours with 700 kW of operating proton beam power.

2. Experimental section

2.1. Calculation of the distance of the SO_3^- Sites ($l_{SO_3-SO_3}$)

By using L_{Cubic} = 9.69 nm and the film density of 1.20 g cm^{-3} when the water content of **Film-G** is 16.4 wt% (Fig. S3),[1] the number of the **GZ** molecules in a cubic cell is calculated to be about 502 (Table. S1). Thus, about 1004 of the SO_3^- groups sit on a gyroid minimal surface (G-surface) in a cubic unit cell. The area of the G-surface in a cubic cell can be calculated from $L_{Cubic}^2 \times 3.09 = 290\ nm^2$ (Fig. S3).[4] By using these values and assuming that the SO_3^- groups are homogenously dispersed on the G-surface, $l_{SO_3-SO_3}$ in **Film-G(16.4)** can be roughly estimated to be 5.8 Å (Fig. S4). This value is predominantly smaller than that of Nafion. This is a value for which one can expect the exhibition of ultrafast SPHC with very small E_a.

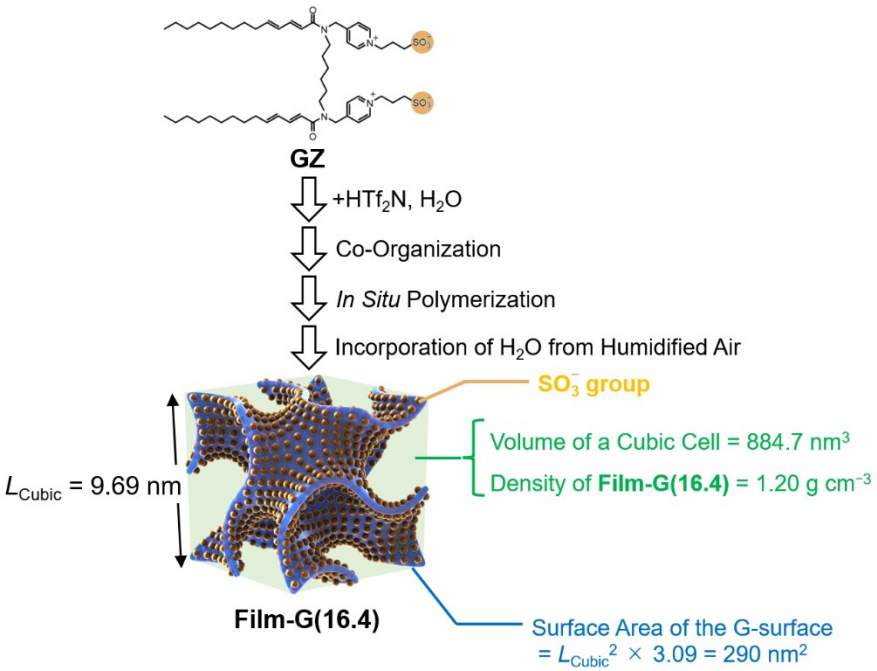

Fig. S3. The volume and density of a cubic cell in **Film-G(16.4)**. The surface area of G-surface is also shown.

Table S1. The weight of each component in a cubic cell and the number of component molecules in the cubic cell

	GZ	**HTf_2N**	**H_2O**
Molecular weight	955.37	281.14	18.02
Molar ratio	1	0.5	11.93
Percentage by weight	72.88	10.72	16.40
The weight of each component in a cubic unit cell (g)	7.96×10^{-19}	1.17×10^{-19}	1.79×10^{-19}
The number of component molecules in a cubic unit cell	502	251	5984

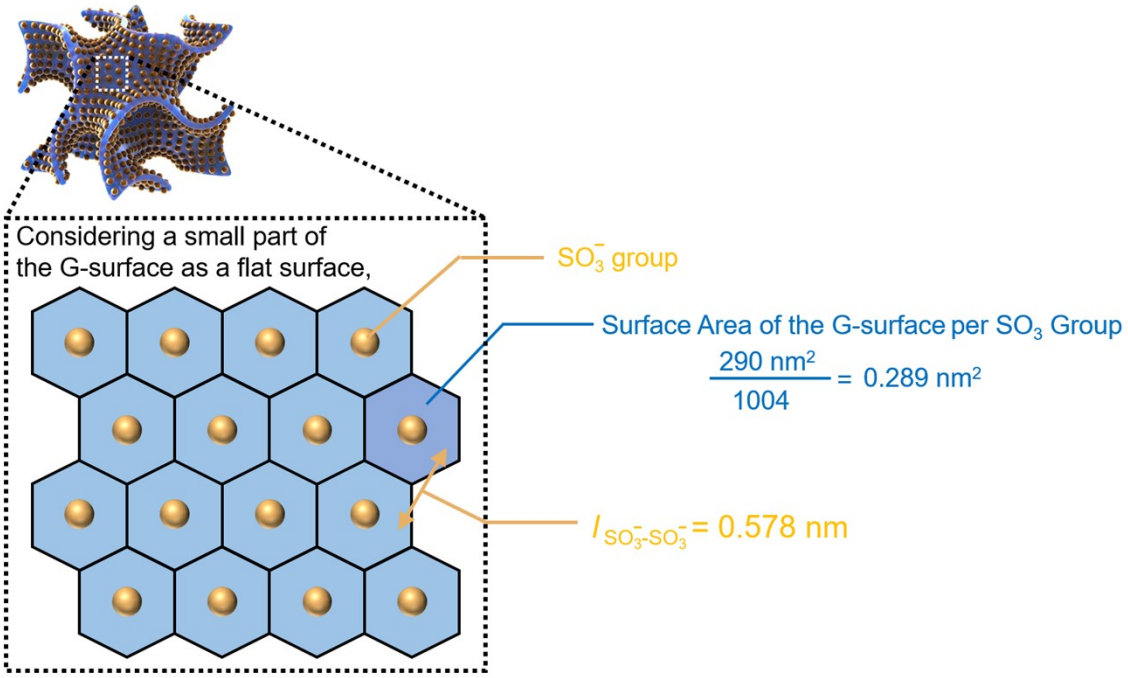

Fig. S4. Rough estimation of $l_{SO_3^- - SO_3^-}$ with considering that a small part of the G-surface is a flat surface and the SO_3^- groups form a hexagonal distribution on the flat surface. For the estimation of $l_{SO_3^- - SO_3^-}$, the number of the SO_3^- groups on the G-surface and the area of the G-surface in a cubic cell is used.

2.2. Ionic conductivity of Film-G

Alternating current impedance measurements were performed for **Film-G** containing X wt % of water (X = 15.2, 9.9, and 6.0) at various temperature. Cole-Cole plots for **Film-G(X)** at 30 °C are shown in Fig. S5. The σ_{H^+} values were calculated using the cell constant value of 0.764 [cm^{-1}] shown in page S3.

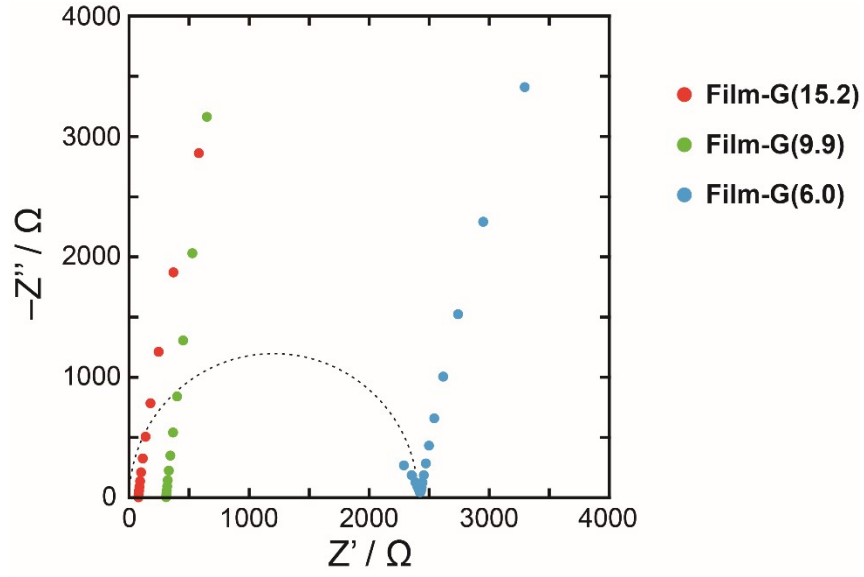

Fig. S5. Cole-Cole plots for **Film-G** containing X wt % of water (X = 15.2, 9.9, and 6.0) at 30 °C.

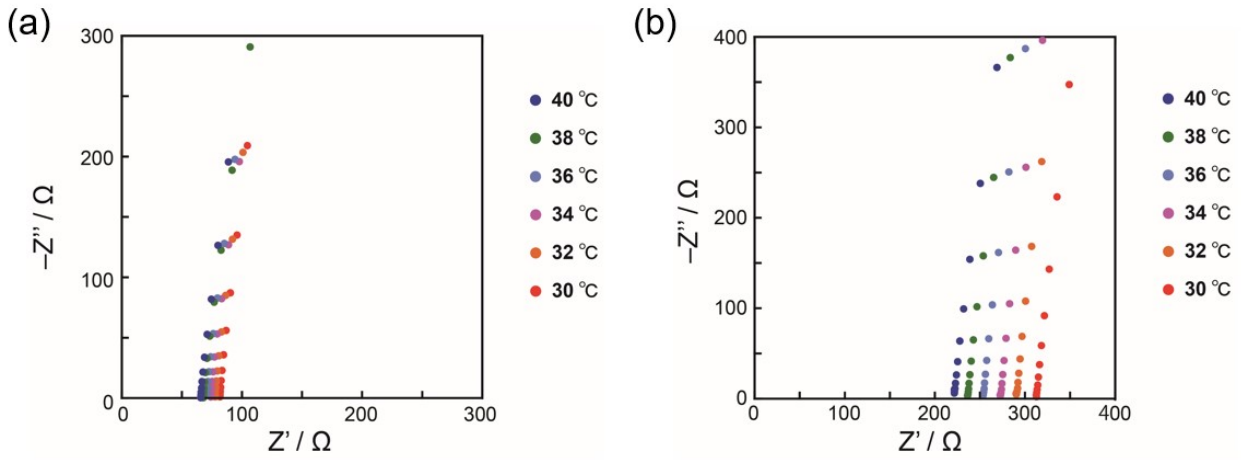

Fig. S6. (a) Cole-Cole plots for **Film-G** containing 15.2 wt % of water at various temperature. (b) Cole-Cole plots for **Film-G** containing 9.9 wt % of water at various temperature.

To examine the temperature dependence of σ_{H^+} is a useful strategy for evaluating the apparent activation energy (E_a) of proton conductive materials. In the case of Nafion, it is generally understood that experimentally obtained E_a values for wet Nafion are largely related with solvent-re-organization energy while those obtained for highly-dried Nafion are attributed to a large electrostatic potential barrier that the protons on the surface have to overcome. We examined the temperature dependence of the ionic conductivity (σ) for **Film-G(X)**. The σ values were measured using two rod-shaped gold electrodes. Since the dominant carrier ion in **Film-G(X)** is H^+, we approximated σ_{H^+} with σ. The logarithm of the obtained σ_{H^+} values are plotted against the reciprocal of absolute temperature. The activation energy (E_a) was estimated from the slope of the plots in the lower temperature range of 30-40 °C in order to suppress the possibility of the evaporation of the absorbed water.

2.3. Estimation of various parameters

2.3.1. Estimation of ε_i (volume fraction occupied by water)

The volume fraction occupied by water, ε_i, was estimated as below. Firstly, we examined the change of the volume of a cubic unit cell before and after water absorption. The cubic lattice length was evaluated from X-ray diffraction results in our previous study.[1] The difference of the volume of the unit cell between **Film-G(16.4)** and **Film-G(1.2)** was 9.69^3 nm^3 – 8.97^3 nm^3 (Fig. S7). By dividing this value with 9.69^3 nm^3, the volume percentage where water occupy was calculated to be 20.6 %. This value is comparable to the increase of the water content weight ratio (16.4 – 1.2 = 15.2 wt%). These results suggest that ε_i (%) can be approximated by the water content X value.

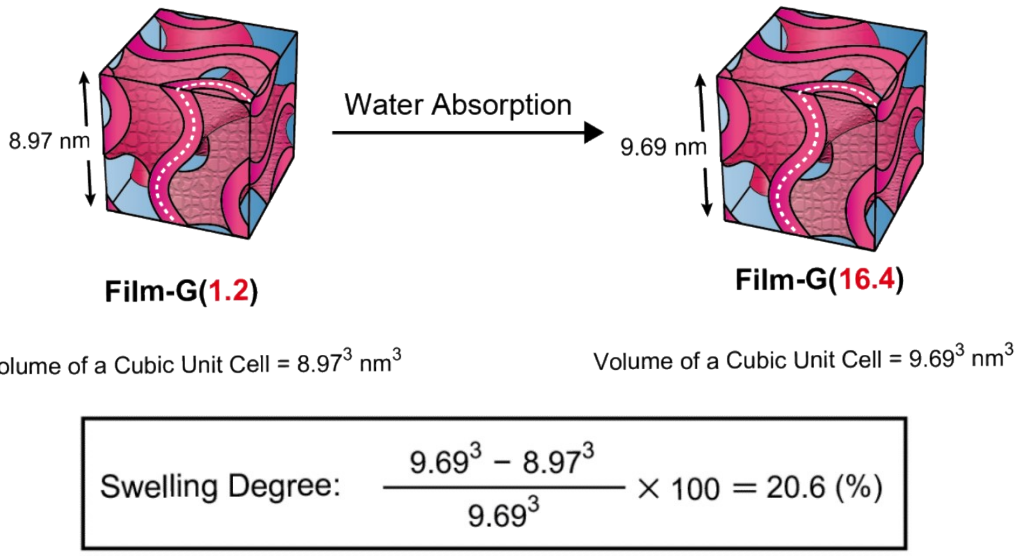

Fig. S7. The difference of the volume of a cubic unit cell before and after water absorption that is calculated from the cubic lattice length obtained from X-ray diffraction measurements.[1]

2.3.2. Estimation of $C_{H^+}^{\Sigma}$ (concentration of proton)

It is assumed that the density of the 3D water nanosheet on the gyroid minimal surface is not far from that of bulk water. Therefore, we consider it as 1 g cm^{-3}. Based on this idea, concentration of proton, $C_{H^+}^{\Sigma}$, can be evaluated from the number of water molecules per H^+ in the 3D water nanosheet (Table S2). The number of H^+ is calculated by assuming that all of HTf_2N molecules in **Film-G** are in the dissociated state. Comparing the molar ratio of H^+ and H_2O in **Film-G(15.2)** with that in a 1 M of an acid solution (Table S3), the concentration of proton in the 3D water nanosheet in **Film-G(15.2)** can be calculated to be 2.54 (M) as below.

$$\frac{55.49}{10.90} \times 0.5 = 2.54 \text{ (M)}$$

Table S2. The molar ratio of **GZ**, HTf_2N, and H_2O in **Film-G(15.2)**

	GZ	HTf_2N	H_2O
Molecular Weight	955.37	281.14	18.02
Molar Ratio	1.00	0.50	10.90

Table S3. The molar ratio of H_2O and H^+ in a 1 M of an acid solution

	H_2O	H^+
Molecular Weight	18.02	1.00
Mole in a 1L acid solution (1 M)	55.49	1.00
Molar Ratio	55.49	1.00

2.3.4. Estimation of l_{Σ} (hopping length)

In the case of conventional Grotthuss mechanism, l_{Σ} is usually considered to be 0.255 nm based on the O-O distance in the hydrated proton forms. In the present study, we propose a SPHC conduction model shown in Fig. 3d where H^+ moves 0.59 nm via two hops. Therefore, it is reasonable to consider l_{Σ} as the half of 0.59 nm, namely 0.295 nm.

2.3.5. Estimation of θ (tortuosity)

Tortuosity (θ) of proton conduction pathways usually depends on the volume fraction occupied by water (ε_i). Estimation methods for θ have been proposed by several groups.[5-7] For example, in the case of general polymer electrolytes, it can be predicted by using percolation theory.[8,9] However, in the case of **Film-G**, the proton conduction pathway is formed along a G-surface that continues in XYZ directions infinitely, meaning that there is no need to apply percolation theory. Our idea for estimating θ in **Film-G** is that it is roughly estimated by calculating the ratio of the curve length along a sine curve against the cubic lattice length, which is 7.64/2π = 1.21 (Fig. S8).

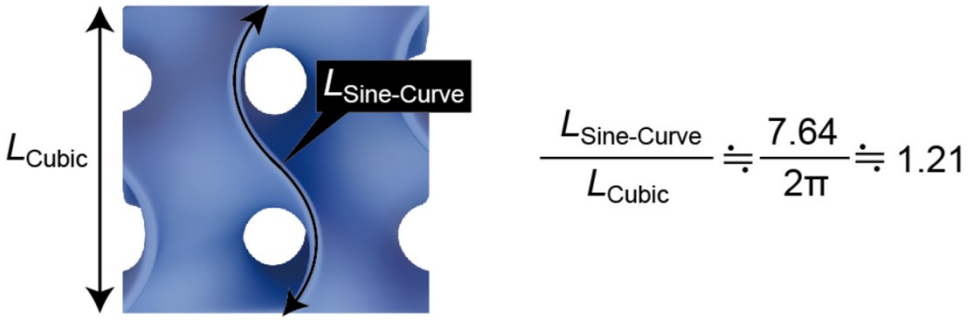

Fig. S8. The tortuosity (θ) of a gyroid minimal surface.

2.3.6. Estimation of κ (a constant value that depends on the dimensionality of random walk)

κ is a constant value that depends on the dimensionality of random walk. It can be regarded as 2, 4, or 6 for a one-, two-, or three-dimensional walk, respectively. In the case of 2D nanochannel models, proton hops from a SO_3^- site to a neighboring water molecule in a direction perpendicular to the hydrophobic walls are thermodynamically unfavorable because the proton receives cooperative electrostatic attractions from several nearby SO_3^- sites. Therefore, proton hops along the hydrophobic wall toward a neighboring SO_3^- site are much more feasible, indicating that it is reasonable to assume κ as 4 (Fig. S9).

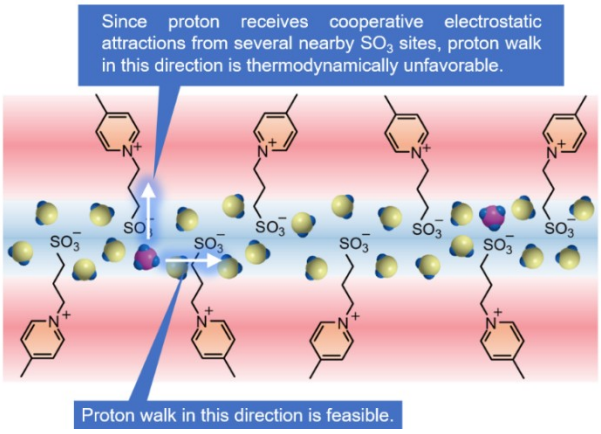

Fig. S9. Dimensionality of proton walk on a gyroid minimal surface in **Film-G**.

2.3.7. Estimation of $^{\Delta G^{e,0}_{\Sigma}}$ (the effective Gibbs free energy of activation)

Assuming that the proton conduction in Film-G is dependent solely on surface proton hopping conduction mechanism, $^{\Delta G^{e,0}_{\Sigma}}$ in **Film-G(X)** was estimated based on the experimentally-obtained $^{\sigma_{H^+}}$ values at 30 °C and the various parameters summarized in Table S4. The estimated $^{\Delta G^{e,0}_{\Sigma}}$ values are summarized in Table. S5. They are compared with E_a values. It was found that there is a large difference between the estimated $^{\Delta G^{e,0}_{\Sigma}}$ values and E_a values while the difference becomes small as the increase of the water content X. It can be explained by the change of the surface proton hopping conduction mechanism as shown in Fig. 3a-d. The difference between the $^{\Delta G^{e,0}_{\Sigma}} = 13.3$ kJ mol^{-1} and $E_a = 17.2$ kJ mol^{-1} can be explained as below. When estimating the E_a values, the relative humidity was controlled to be 90%. As the increase of temperature, the absolute humidity increases, which leads to a slight increase of the water content in **Film-G(15.2)**. Therefore, the slope in the Arrhenius plot appears as a slightly-larger value than the exact activation energy. Therefore, the slight difference is acceptable and reasonable.

Table S4. Various parameters that are used for the calculation of $^{\Delta G^{e,0}_{\Sigma}}$

Parameter	Value	Unit
$v_0 = \frac{k_B T}{h}$	6.418×10^{12}	s^{-1}
h	6.626070×10^{-34}	m^2 kg s^{-1}
k_B	1.380649×10^{-23}	J K^{-1}
T	303	K
Avogadro constant N_A	6.02214×10^{23}	mol^{-1}
l_Σ	0.295	nm
κ	4	dimensionless
ε_i	0.164	dimensionless
θ	1.21	dimensionless
F	96485	C mol^{-1}
R	8.314	J K^{-1} mol^{-1}
T	303	K
$^{C^{\Sigma}_{H^+}}$ (mol/L)	2.326	mol L^{-1}
$^{C^{\Sigma}_{H^+}}$ (mol cm^{-3})	2.326×10^{-3}	mol cm^{-3}

Table S5. Activation energy and ionic conductivity of **Film-G** containing X wt% of water

	$^{\sigma_{H^+}}$ at 30 °C (S cm^{-1})	Estimated $^{\Delta G^{e,0}_{\Sigma}}$ (kJ mol^{-1})	E_a values (kJ mol^{-1})
Film-G(6.0)	5.37×10^{-4}	20.4	35.3
Film-G(9.9)	2.21×10^{-3}	16.8	27.1
Film-G(15.2)	8.45×10^{-3}	13.3	17.4

2.3.8. Estimation of $^{\Delta}\tau_{D(App)}^{\Sigma}$ (mean jump time for a proton hop)

$\tau_{D(App)}^{\Sigma}$ of **Film-G(15.2)** at various temperatures were calculated using the value of $\Delta G_{\Sigma}^{e,0} = 13.3\ kJ/mol$ (Table S6).

Table S6. $\tau_{D(App)}^{\Sigma}$ of **Film-G(15.2) at various temperatures**

Temperature (K)	$\tau_{D(App)}^{\Sigma}$ (s)
300	32.5×10^{-12}
280	50.9×10^{-12}
260	84.9×10^{-12}
240	153.3×10^{-12}

2.4. Characterization of the state of water molecules in Film-G

2.4.1. Our assumption on the existence position of water molecules

Here we note that the zwitterion part of **GZ** has an ability to form ion exchange with HTf_2N according to the hard and soft, acids and bases principle.[10] Therefore, the molecular assembled nanostructures of the mixture of **GZ**/HTf_2N/water before and after polymerization are expected to be as illustrated in Fig. S10. Since the combination of the pyridinium cation and the Tf_2N anion is a representative ion pair that forms hydrophobic ionic liquids, it is expected that the most of the water molecules locate at around the SO_3^- groups.

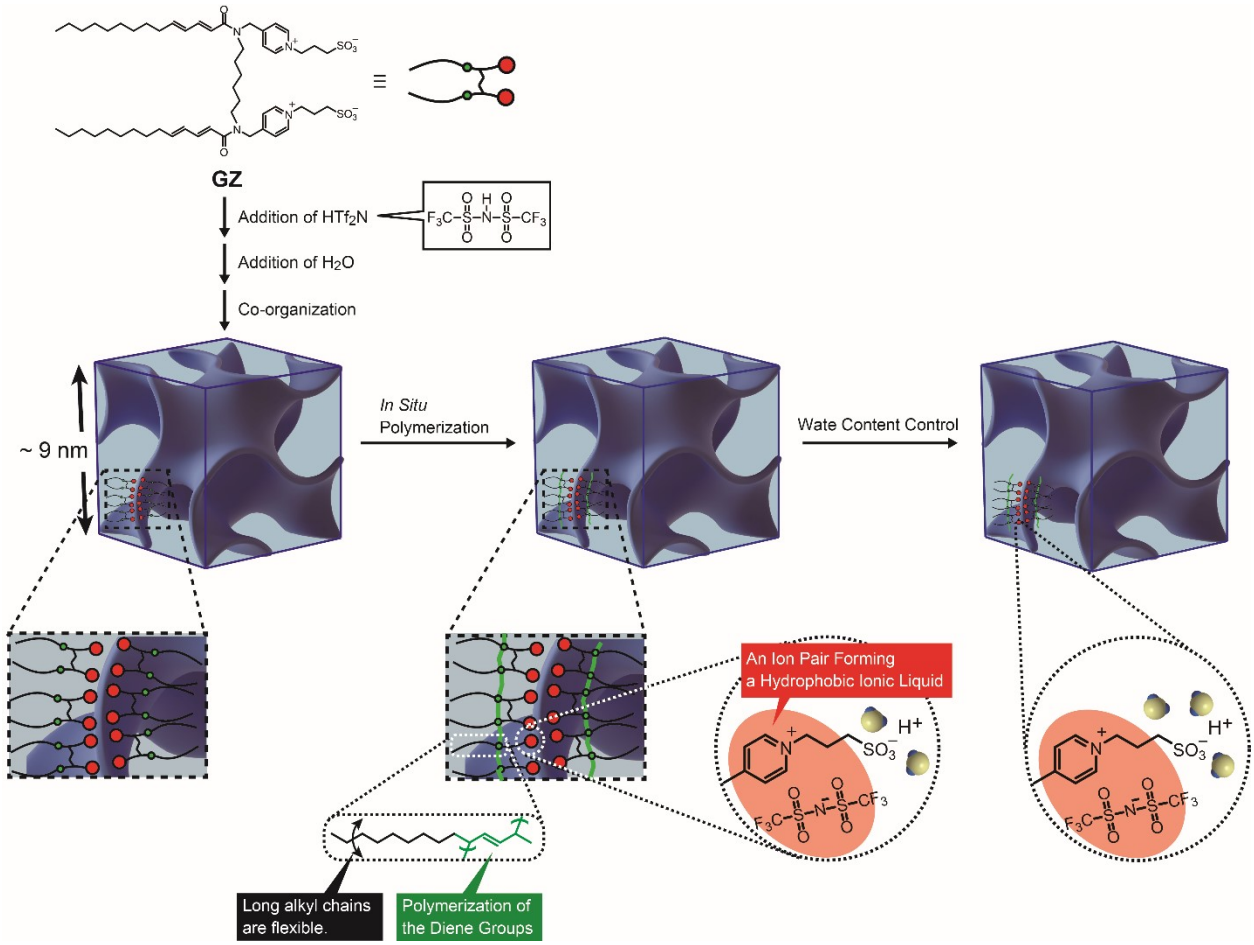

Fig. S10. A schematic illustration of the molecular assembled nanostructure of **GZ** in the presence of HTf_2N and water.

2.4.2. State of water molecules in Film-G(X)

DSC measurements were performed for **Film-G(X)** containing various water content X. The heating and cooling rates were 5 °C min^{-1}. The data on cooling are shown in Fig. 5 while those on heating are shown in Fig. S11. It was found that **Film-G(X)** show no exothermic and endothermic peak on heating when $X \leq 15.6$. These results indicate that all of the water molecules in the film exist as non-freezing bound water when $X \leq 15.6$. It is mainly attributed to the strong hydration

ability of the SO_3^- groups although a part of the water molecules is expected to interact with the other ionic species, such as the pyridinium cations of **GZ** and the Tf_2N anion of HTf_2N.

On the other hand, when $X \geq 17.3$, some exothermal and endothermal peaks were found for **Film-G(X)** on heating. For example, **Film-G(17.3)** shows an exothermic and an endothermic peaks on heating. The exothermic peak corresponds to a cold crystallization. Generally, it is expected that the water molecules in this kind of polymer electrolytes can be classified into three classes, free water, freezing bound water, and non-freezing bound water. The numbers of water molecules in each class were calculated as shown in Table S7. For the calculation of the number of freezing bound water per **GZ**, the enthalpy of water melting (334 J g^{-1}) was used. It can be seen that the number of non-freezing bound water per **GZ** is lower than 13, namely the number of non-freezing bound water per SO_3^- group is lower than 6.5. Considering the general insights that these ionic groups have ability to catch about 7 water molecules as bound water,[11] our conclusion can be considered to be objectively valid.

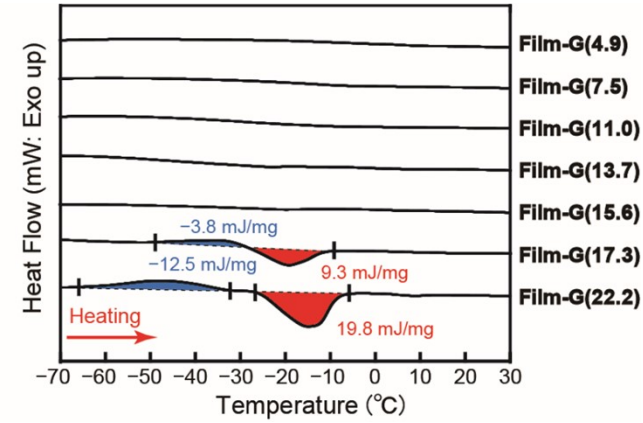

Fig. S11. DSC thermograms of **Film-G(X)** on heating.

Table S7. Molar ratio of **GZ** : HTf_2N : H_2O in **Film-G** and the numbers of free water, freezing bound water, and non-freezing bound water per **GZ**

	Molar ratio of **GZ** : HTf_2N : H_2O	Number of free water per **GZ**	Number of freezing bound water per **GZ**	Number of non-freezing bound water per **GZ**
Film-G(4.9)	1 : 0.5 : 3.1	0	0	3.1
Film-G(7.5)	1 : 0.5 : 4.9	0	0	4.9
Film-G(11.0)	1 : 0.5 : 7.5	0	0	7.5
Film-G(13.7)	1 : 0.5 : 9.7	0	0	9.7
Film-G(15.6)	1 : 0.5 : 11.2	0	0	11.2
Film-G(17.3)	1 : 0.5 : 12.8	0	2.0	10.7
Film-G(22.2)	1 : 0.5 : 17.4	0	4.6	12.7

3. QENS experiments

3.1.1. Preparation of samples for QENS experiments

The precise estimation of the water contents in the samples for QENS experiment is quite important for precise analysis. In order to estimate the water content in the samples, we took the process as explained in Fig. S12. As an example, we explain the case for **Film-G** containing H_2O. First, we prepared four of circle-shaped **Film-G** samples whose weight is about 10-13 mg. The total weight is about 50 mg, which changes depending on relative humidity. In order to obtain the weight of the samples without water, we dried the samples in vacuum. The weight of the four films in the driest state is 46.24 mg. The dried films were placed under a H_2O-humidified condition. The samples were took out when the total weight of the four films reached 50.80 mg. The water content in the films was calculated to be 4.56 mg. As well as the **Film-G** samples containing H_2O, those containing D_2O were prepared in the same procedure. The calculation of the molar ratio is explained in **3.2.** in the next page.

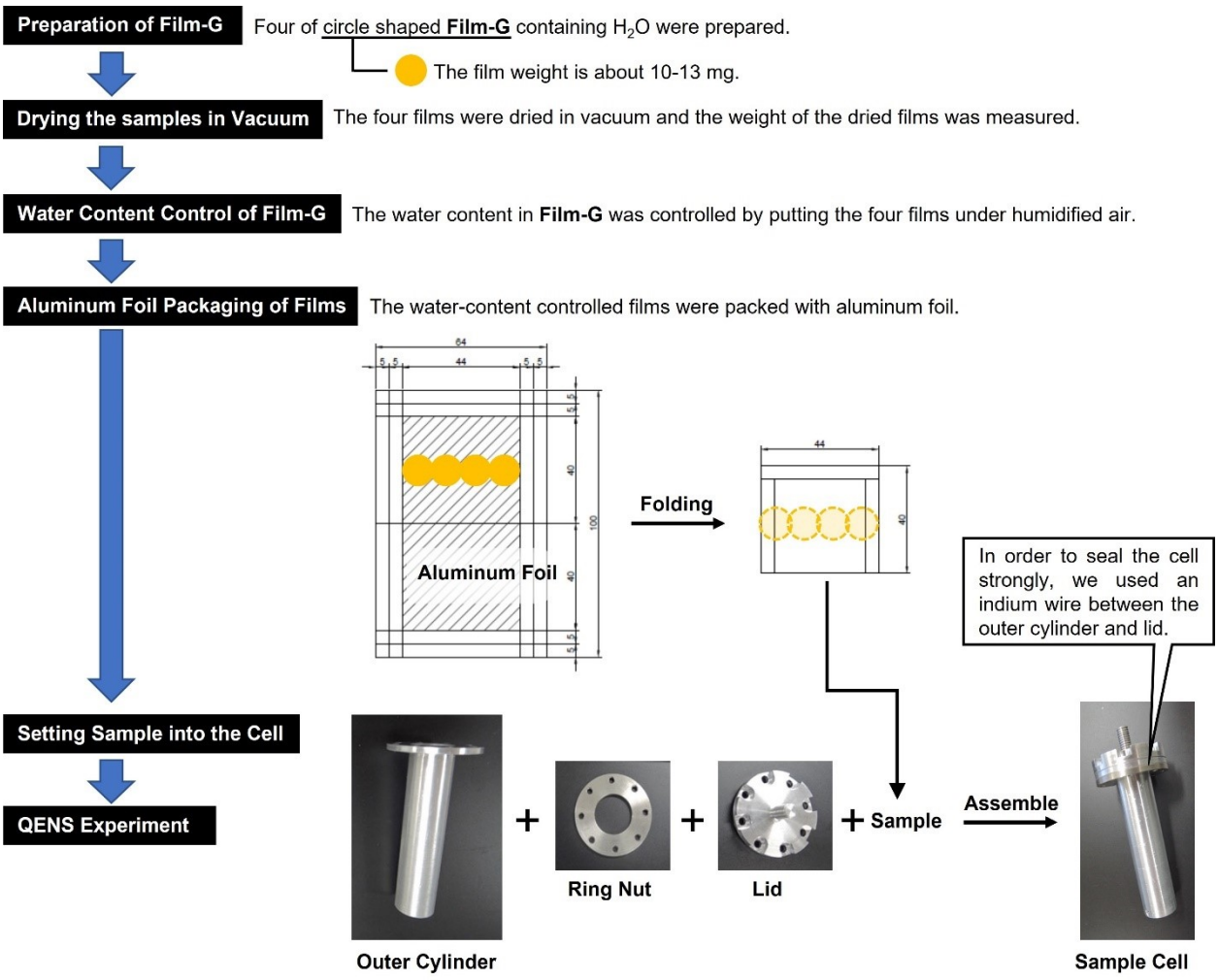

Fig. S12. Preparation procedure of the samples for QENS experiment. **Film-G** containing H_2O was prepared according to the procedure. **Film-G** containing D_2O was also prepared in the same way.

3.1.2. Details of samples

Calculation of the molar ratio of **GZ**, HTf_2N, and H_2O in **Film-G** was carried out as summarized in Table S8 and Table S9. The total weight of four of circle shaped **Film-G** containing H_2O is 50.80 mg (Table S8). The molar ratio of **GZ**, HTf_2N, and H_2O is calculated to be 1.00:0.50:6.00 (Table S9), indicating that there are about 6 water molecules per **GZ** molecule (3 water molecules per zwitterion).

Table S8. Water content in **Film-G** containing H_2O

	Film-G containing H_2O
Total weight of **Film-G** containing H_2O (mg)	50.80
Weight of **Film-G** in a highly dried state (mg)	46.24
Weight of H_2O in **Film-G** (mg)	4.56
Water content in **Film-G** (wt%)	8.98

Table S9. The molar ratio of **GZ**, HTf_2N, and H_2O

	GZ	HTf_2N	H_2O	Total
Weight of each component (mg)	40.31	5.93	4.56	50.80
Molecular Weight	955.37	281.14	18.02	-
Mole of each component (mmol)	0.0422	0.0211	0.253	-
Molar Ratio	1	0.50	6.00	-

3.2.2. Characterization of Film-G containing $3D_2O$

Calculation of the molar ratio of **GZ**, HTf_2N, and D_2O in **Film-G** was carried out as summarized in Table S10 and Table S11. The total weight of four of circle shaped **Film-G** containing D_2O is 53.00 mg (Table S10). The molar ratio of **GZ**, HTf_2N, and D_2O is calculated to be 1.00:0.50:5.95 (Table S11), indicating that there are about 6 water molecules per **GZ** molecule (3 water molecules per zwitterion).

Table S10. Water content in **Film-G** containing D_2O

	Film-G containing D_2O
Total weight of **Film-G** containing D_2O (mg)	53.00
Weight of **Film-G** in a highly dried state (mg)	47.80
Weight of D_2O in **Film-G** (mg)	5.20
Water content in **Film-G** (wt%)	9.81

Table S11. The molar ratio of **GZ**, HTf_2N, and D_2O

	GZ	HTf_2N	D_2O	Total
Weight of each component (mg)	41.67	6.13	5.20	53.00
Molecular Weight	955.37	281.14	20.03	-
Mole of each component (mmol)	0.0436	0.0218	0.259	-
Molar Ratio	1	0.50	5.95	-

3.1.3. Details of samples

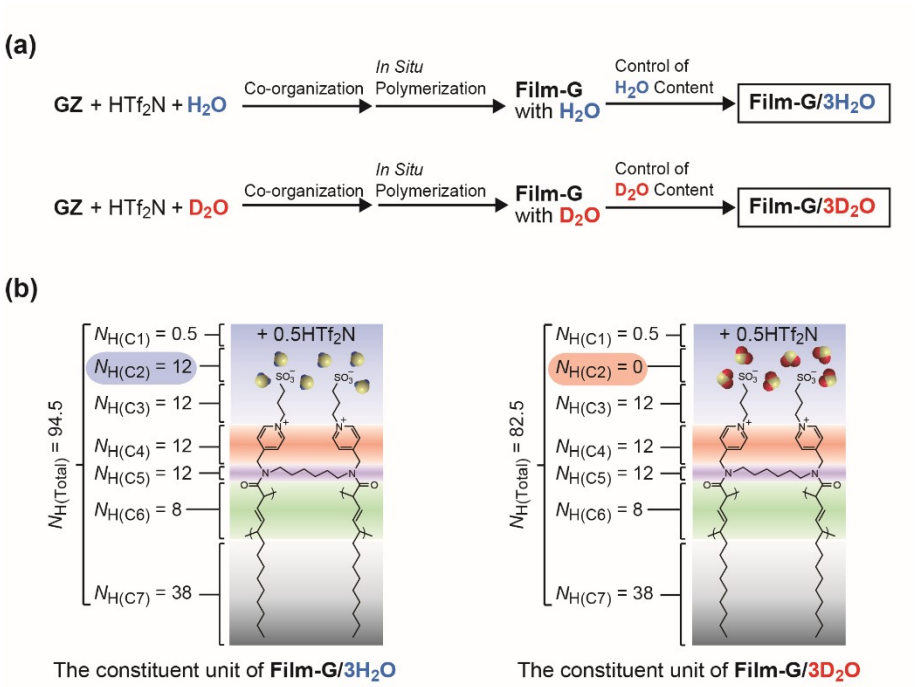

Fig. S13. (**a**) Preparation schemes for the two types of **Film-G** containing H_2O or D_2O. The co-organization of **GZ**, HTf_2N, and H_2O (or D_2O) and the subsequent *in situ* polymerization yielded **Film-G** containing a certain amount of H_2O or D_2O. Since the water contents slightly change during the polymerization process, the water contents were controlled after the polymerization by drying in a vacuum and subsequent gradual absorption of a controlled amount of water (H_2O or D_2O) from humidified air. (**b**) The numbers of the hydrogen atoms ($N_{H(Cm)}$) in each class of the constituent units of **Film-G/3H_2O** and **Film-G/3D_2O**.

Two types of **Film-G** samples containing H_2O or D_2O were prepared according to the scheme shown in Fig. S13a. The water contents in the samples were adjusted to be about 9.0 and 9.8 wt%, respectively, by putting them under controlled relative humidity conditions. Both of the resultant polymer films contain 3.0 water molecules (H_2O or D_2O) per zwitterion part. Below they are described as **Film-G/3H_2O** and **Film-G/3D_2O**, respectively. Taking into account the constituent unit of **Film-G/3H_2O** is comprised of 1.0**GZ**, 0.5HTf_2N, and 6H_2O molecules, we roughly classify the hydrogen atoms in the constituent unit into 7 classes as shown in Fig. S13b. For example, the numbers of hydrogen atoms in each class of **Film-G/3H_2O** ($N_{H(Cm)}$, m = 1-7) are 0.5, 12, 12, 12, 12, 8, and 38 in this order. The total of hydrogen atoms ($N_{H(Total)}$) is 94.5. Based on the number of the hydrogen atoms in these classes, we discuss the QENS results in the following paragraphs.

3.2. Analysis of QENS results

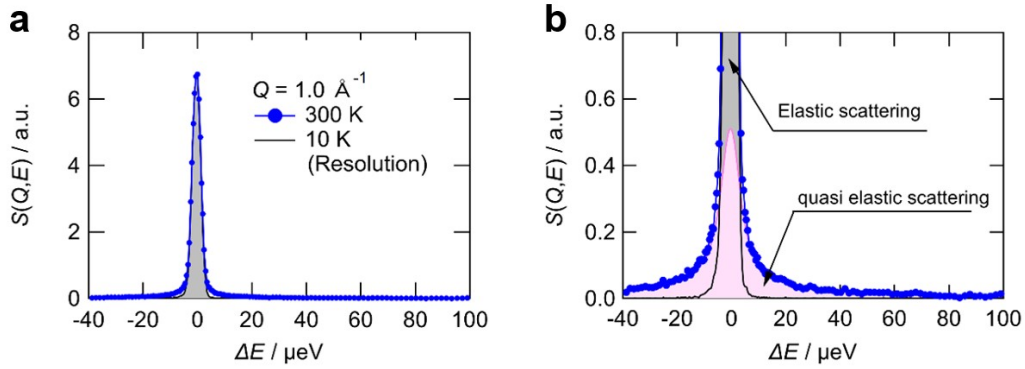

Fig. S14. a, QENS profiles of **Film-G/3H$_2$O** at Q = 1.0 Å^{-1} at 300 K (blue circles) and 10 K (gray shaded part). **b**, 10 time magnification of y-axis of [**a**].

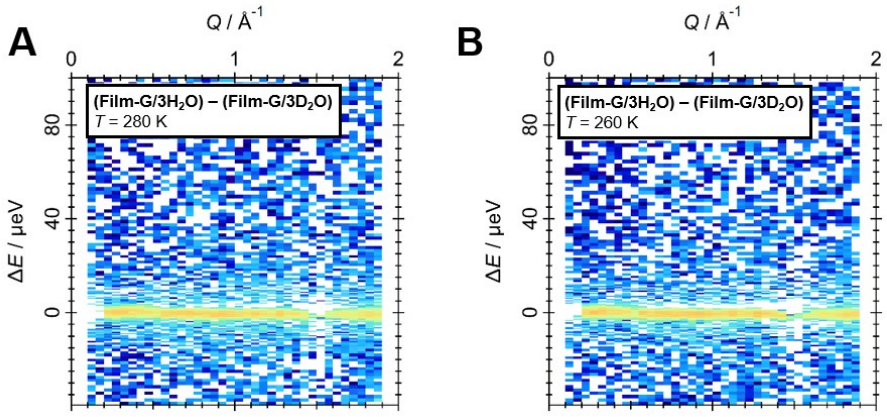

Fig. S15. The differential counter maps between (**Film-G/3H$_2$O**) and (**Film-G/3D$_2$O**) at 280 K (left) and 260 K (right). The white parts corresponding to negative values appeared at around ΔE = 0.

3.3. Detailed analysis of QENS results

As mentioned in the main text, QENS profile of **Film-G/3D$_2$O** reflects the dynamics of **Film-G** under the hydrated state because the D_2O hardly influence the QENS profile due to the much smaller incoherent scattering cross section of deuterium than that of hydrogen. The QENS data shown in Fig. 6b (**Film-G/3D$_2$O**) was divided into 12 QENS profiles with width of 0.15 Å^{-1}. The profiles were well reproduced by Eq. 6 with two Lorentz function (n = 2). Three examples of the 12 profiles are as shown in Fig. S16. The half width at half-height (HWHM) of the Lorentzian components (Γ_1: filled squares, Γ_2 : open squares) in $L_1(\Gamma_1, E)$ and $L_2(\Gamma_2, E)$ are plotted against Q (Fig. S17). These values are almost constant to the Q values. Thus, the observed motions are due to local motion in **Film-G**.

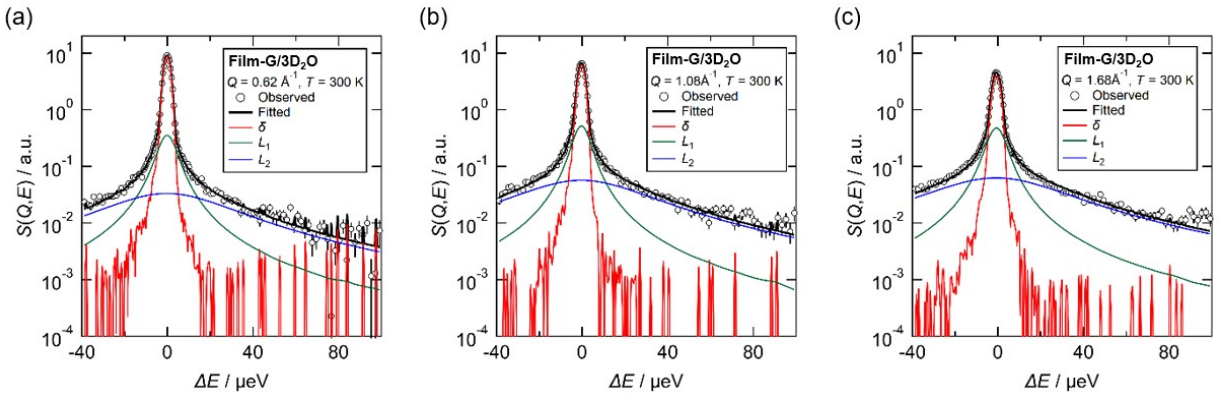

Fig. S16. QENS profiles of **Film-G/3D$_2$O** at (a) Q = 0.62; (b) Q = 1.08; and (c) Q = 1.68 Å^{-1} at 300 K.

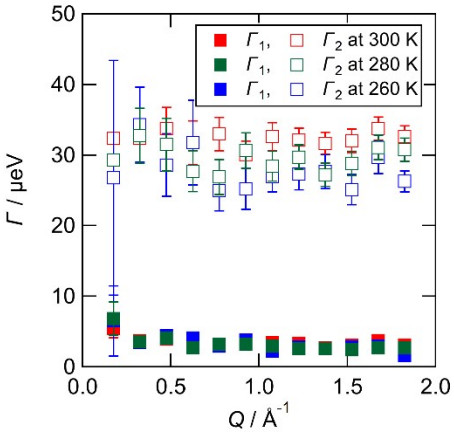

Fig. S17. The half width at half-height maximum (HWHM) of the Lorentzian components (Γ_1: filled squares, Γ_2 : open squares) in $L_1(\Gamma_1, E)$ and $L_2(\Gamma_2, E)$ versus Q for **Film-G/3D$_2$O** at 300 (red), 280 (green), and 260 K (blue).

Elastic incoherent scattering factors (EISFs)[12] were calculated using the obtained A_0, A_1, and A_2 values as follows,

$$EISF = \frac{A_0}{A_0 + A_1 + A_2}$$

The obtained EISFs were plotted against Q (Fig. S18). The EISFs were approached to unity at $Q \rightarrow 0$ and it is also characteristics of local mode. The EISF at Q = 1.82 Å^{-1} at 300K suggest that about 55 % of the hydrogen atoms exist as the elastic components while the remain (45 %) is dynamic (Fig. S18). Considering that the number of the hydrogen atoms in the long alkyl chain parts, $N_{H(C7)}$, is 38, which corresponds to 46 % of the whole ($N_{H(Total)}$ = 82.5) (Fig. S13b), it is reasonable to assume that the two quasi elastic components, A_1 and A_2, is mostly attributed to the long alkyl chain parts in **Film-G**. The EISF increased and the Γ_2 decreased with decreasing temperature. It could be due to the slowing down of the alky chain, so that some QENS parts changed into the elastic. In this analysis, the dynamics of the alkyl chain is simplified by two relaxational components while it could be more complex. As a result, the analysis may catch characteristic modes in the measured energy transfer window, and temperature dependence of the width (Γ_1) was not observed.

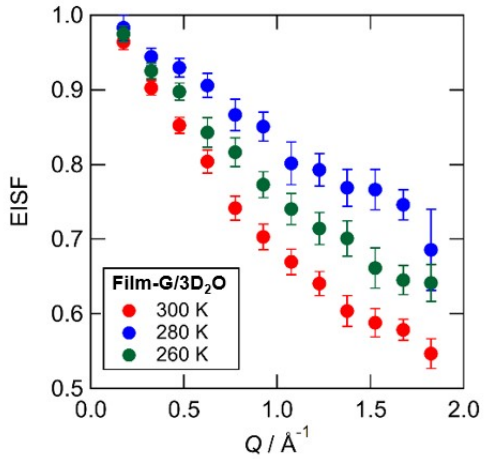

Fig. S18. Q dependence of the elastic incoherent structure factor (EISF) of **Film-G/3D$_2$O** at 300, 280, and 260 K.

The QENS data of **Film-G/3H$_2$O** was also grouped into 12 QENS profiles. The same analysis procedure was applied to these data on the condition that the parameters obtained from **Film-G/3D$_2$O** was fixed and A_0, A_3, Γ_3 were fitting parameters. A typical fitting result was shown in Fig. S19a. The QENS profile was also well reproduced. The EISF of the absorbed water corresponding to C2 in Fig. S13b ($EISF_{(C2)}$) was calculated by (eq. 10) without multiplying 12 in eq.7.

$$EISF_{(C2)} = \frac{A_0(Film - G/3H_2O) - A_0(Film - G/3D_2O)}{\left(A_0(Film - G/3H_2O) - A_0(Film - G/3D_2O) + A_3\right)} \quad \text{(Eq. 10)}$$

The obtainedΓ_3 and $EISF_{(C2)}$ were shown in Fig. S19b. Although the both Γ_3 and $EISF_{(C2)}$ were scattered and had large error bars due to the inadequate statistics due to the increase of Q points,

the Γ_3 values were almost constant and the $EISF_{(C2)}$ values were approached to unity at $Q \rightarrow 0$, so that the observed dynamics of the absorbed water could be local mode (rotation and/or jump). The number of the mobile hydrogen atom estimated from the averaged EISF (0.84 ± 0.06) was 1.9 ± 0.7, which is also roughly consistent with the result in Fig. 8a.

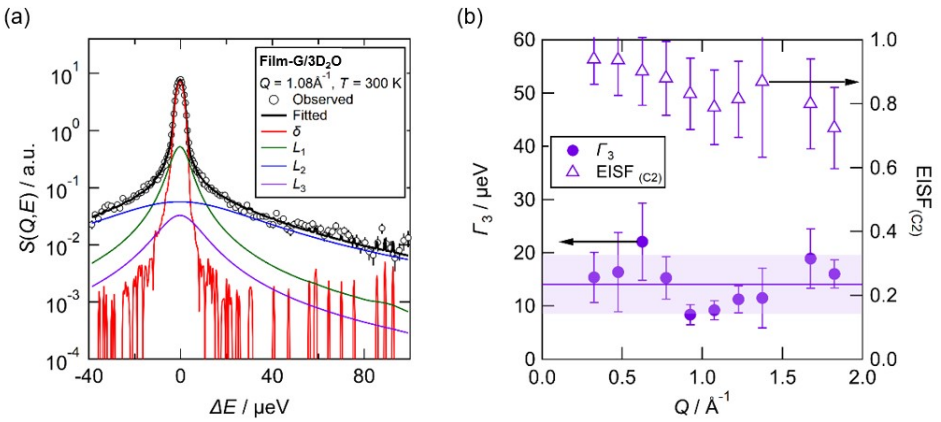

Fig. S19. a, Fitting of the 12 divided QENS profile of **Film-G/3H$_2$O** at Q = 1.08 Å^{-1} at 300 K when the parameters of two Lorentzian-functions were fixed by the results of **Film-G/3D$_2$O**. **b**, Plot of Γ_3 and $EISF_{(C2)}$ versus Q for **Film-G/3H$_2$O** at 300 K.

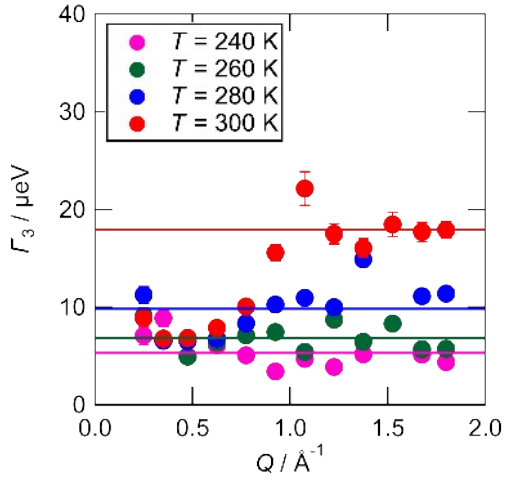

Fig. S20. Q dependence of Γ_3 of **Film-G/6H$_2$O** at various temperatures.

4. References

1. T. Kobayashi, Y. Li, A. Ono, X. Zeng, T. Ichikawa, *Chem. Sci.* **10**, 6245–6253 (2019).
2. K. Shibata, N. Takahashi, Y. Kawakita, M. Matsuura, T. Yamada, T. Tominaga, W. Kambara, M. Kobayashi, Y. Inamura, T. Nakatani, K. Nakajima, M. Arai, *JPS Conf. Proc.* **8**, 036022 (2015).

3. H. Seto, S. Itoh, T. Yokoo, H. Endo, K. Nakajima, K. Shibata, R. Kajimoto, S. Ohira-Kawamura, M. Nakamura, Y. Kawakita, H. Nakagawa, T. Yamada, *Biochim. Biophys. Acta - General Subjects* **1861**, 3651–3660 (2017).
4. O. Al-Ketan, R. K. Abu Al-Rub, *Adv. Eng. Mater.* **21**, 1900524 (2019).
5. S. Prager, *J. Chem. Phys.* **33**, 122 (1960).
6. H. Yasuda, E. Lamaze, and L. D. Ikenberry, *Makromol. Chem.* **118**, 19–35 (1968).
7. S. Koter, *J. Membr. Sci.* **206**, 201–215 (2002).
8. W. Y. Hsu, J. R. Barkley, P. Meakin, *Macromolecules* **13**, 198–200 (1980).
9. B. Ghanbarian, A. G. Hunt, M. Sahimi, R. P. Ewing, T. E. Skinner, *Soil Sci. Soc. Am. J.* **77**, 1920 (2013).
10. R. G. Pearson, *J. Am. Chem. Soc.* **85**, 3533–3539 (1963).
11. H. Ohno, K. Fujita, Y. Kohno, *Phys. Chem. Chem. Phys.* **17**, 14454–14460 (2015).
12. M. Bée, *Phys. B* **182**, 323–336 (1992).